# SCIENTIFIC REPORTS

# The microscopic origin of the extreme glass-forming ability of Albite and $B_2O_3$

Edgar D. Zanotto & Daniel R. Cassar

Understanding the conditions that favour crystallisation and vitrification has been a longstanding scientific endeavour. Here we demonstrate that the extremely high glass-forming ability of unseeded supercooled $Na_2O \cdot Al_2O_3 \cdot 6SiO_2$ (Albite) and $B_2O_3$—known for decades as "crystallisation anomaly"—is caused by insufficient crystal nucleation. The predicted temperatures of the maximum homogeneous nucleation rates are located well below their glass transition temperatures ($T_g$), in a region of very high viscosity, which leads to extremely long nucleation time-lags and low nucleation rates. This behaviour is due to the remarkably small supercoolings where the glass transition occurs for these liquids, which correspond to a very small driving force for crystallisation at and above the $T_g$, where crystallisation is normally observed. This meagre nucleation ability is caused by the significant difference in the structures of the supercooled liquids and their isochemical crystals. These findings elucidate the cause behind the crystallisation anomaly, and could be used for the design of other oxide glasses that are extremely stable against crystallisation.

The most stable thermodynamic state of matter below the melting point or *liquidus* is the crystalline state, where the atoms are well organized in a periodic lattice at short-, intermediate-, and long-range distances. The vast majority of natural materials on Earth's crust are crystalline. To make glasses one has to deceive the natural solidification path: crystallisation[1]. There has been a long-standing quest to understand the conditions that favour crystallisation and vitrification of supercoooled liquids (and the nature of the vitreous state) ever since glasses became a major topic within condensed matter physics and materials science and engineering.

Most ionic, covalent, van der Waals, mixed bonded, metallic, and inorganic liquids crystallise within laboratory time scales when they are cooled down somewhat below their respective equilibrium melting points or *liquidus* temperatures ($T_m$). Turning to the realm of inorganic glasses, researchers and engineers frequently struggle against unwanted spontaneous crystallisation (also known as *devitrification*) when they try to make glasses in their laboratories or industries; whereas others try to design and control crystallisation in glass article interiors to produce a type of nanoporcelain known as *glass-ceramics*[2–4]. In fact, "crystallisation" is so important that it is the most frequent keyword used by researchers in the last 200 years of glass science history[5].

However, to the best of our knowledge and to our great surprise, crystallisation has never been reported to occur in pure <u>unseeded</u> supercooled $Na_2O \cdot Al_2O_3 \cdot 6SiO_2$ (Albite) and $B_2O_3$ liquids, at atmospheric pressure. These materials display outstanding glass-forming ability (when cooled from the liquid state), and are likely the most stable stoichiometric oxides against crystallisation (on heating from the glassy state) discovered to-date! In the glass science field, a "stoichiometric glass" is one that has a thermodynamically stable isochemical crystalline phase. This definition should not be confused with the traditional "stoichiometry", that is, the calculation of relative quantities of reactants and products in chemical reactions.

In this article we will focus on both glasses: in Albite glass because it is also outstandingly chemically durable and may, for instance, provide an excellent matrix for the immobilization of radioactive fission products; and on $B_2O_3$ because this is one of the main oxide glass-formers used in a plethora of commercial glass products. In addition, Albite is a strong liquid, whereas $B_2O_3$ is fragile, and enough information on their structures and properties is available to perform sufficient calculations to develop a strong argument to explain their outstanding glass-forming ability. A liquid may be strong or fragile depending on the value of its fragility index m, defined by

Department of Materials Engineering, Center for Research, Technology and Education in Vitreous Materials, Federal University of São Carlos, São Carlos, SP, Brazil. Correspondence and requests for materials should be addressed to E.D.Z. (email: dedz@ufscar.br)

$m = d\log(\eta(T))/d(T_g/T)\big|_{T=Tg}$, where $\eta$ is the equilibrium viscosity and $T_g$ is the glass transition temperature. Note that this fragility index is not related to the mechanical properties of the material.

As an example of the types of experimental tests performed with these glasses, in the fifties Schairer and Bowen[6] showed how difficult it is to crystallise Albite from its own melt; one sample was held at 1025 °C (close to the temperature of the predicted maximum growth rate) for five years without crystallising[7]. Uhlmann[8] coined the term crystallisation "anomaly" when trying to decipher this unusual behaviour, which that is also shown by $B_2O_3$ glass, which only crystallises after seeding and under very high (GPa) pressures[9]. Albite has been shown to crystallise at atmospheric pressure only when Albite crystal seeds are introduced[10–12]. In a very recent article, Siqueira et al.[13] demonstrated that even a (carbon-free) gel-derived Albite glass—and gels easily devitrify—did not crystallise when heated at the temperature of maximum growth rate. One of us (EDZ) has tried to crystallise an unseeded $B_2O_3$ glass with different thermal treatments without success.

These experiments indicate that the main challenge preventing crystallisation is in the formation (nucleation) of a crystalline phase (Albite and $B_2O_3$), and perhaps even in its growth ($B_2O_3$). This crystallisation anomaly has been a matter of debate for many decades!

The typical stoichiometric oxide glass forming compositions (such as Albite and $B_2O_3$) normally crystallise in laboratory time scales when heated at any temperature somewhat below their melting points and above their $T_g$, and also during non-isothermal DSC (differential scanning calorimetry) runs. However, crystallisation does not occur in Albite and $B_2O_3$ within the time scales of DSC experiments.

Therefore, understanding the reasons why these two glass-formers display this abnormal reluctance to crystallization in heating experiments and outstanding glass-forming ability (in the cooling path from the molten state) is very relevant from the physics, chemistry, and materials science point of view. From a broader scientific perspective, this study could also provide further insight into the nature of the vitreous state and be used for the design of very stable glasses.

In this article we dwell on and calculate three kinetic properties of supercooled liquids that control crystal nucleation and crystal growth: the steady-state homogeneous crystal nucleation rates, $I_{st}(T)$; the nucleation time-lags, $\tau(T)$; and the crystal growth rates, $U(T)$, for Albite and $B_2O_3$. Because the homogeneous nucleation kinetics are too slow to be measured in these liquids, we rely on estimated values of $I_{st}(T)$ and $\tau(T)$. Finally, we use literature data to compare the similarities and differences between the atomic structures of the parent liquids and their isochemical crystal phases. We sought for any thermodynamic, kinetic, or structural signs that could shed light on the lack of observable crystallisation in the supercooled Albite and $B_2O_3$ liquids.

## Thermodynamic and Kinetic Parameters that Control Crystal Nucleation and Growth

Reluctant crystallisation could be due to either exceptionally low steady-state crystal nucleation rates, very long induction periods for nucleation, and/or extremely low crystal growth rates. We will now discuss the governing equations for these three kinetic properties, and at their main controlling parameters, that can be calculated or measured, which are: the crystallisation driving force, the nucleus-melt interfacial energy, and the effective diffusion coefficient. We will then start with a brief definition of these parameters, before discussing the crystal nucleation and crystal growth models.

**Driving Force for Crystallisation ($\Delta\mu$).** Supercooled liquids always have a higher Gibbs free energy ($G_l$) than their stable isochemical crystal phases ($G_c$). The driving force for crystallisation is defined as $\Delta\mu \equiv -\Delta G = G_l - G_c$ and is positive for temperatures below the melting point[14,15]. In addition, the absolute value of $\Delta\mu$ increases with decreasing temperature from the melting point (that is, increasing undercooling). Equation (1) provides a way to calculate $\Delta\mu$ for a closed system under isobaric condition[14,15].

$$\Delta\mu(T) = \Delta H_m\left(1 - \frac{T}{T_m}\right) - \int_T^{T_m}\left(C_{p,l}(T) - C_{p,c}(T)\right)\mathrm{d}T + T\int_T^{T_m}\frac{C_{p,l}(T) - C_{p,c}(T)}{T}\mathrm{d}T \tag{1}$$

In the above equation, $\Delta H_m$ is the molar enthalpy of melting, $C_{p,l}$ is the molar heat capacity of the supercooled liquid, $C_{p,c}$ is the molar heat capacity of the crystal, and $T$ is the absolute temperature. When the driving force for crystallisation is expressed in units of volume rather than in moles of substance, the conversion requires the knowledge of the molar volume, $V_m$:

$$\Delta\mu_V(T) = \frac{\Delta\mu(T)}{V_m}. \tag{2}$$

Figure 1 shows a normalized plot of $\Delta\mu(T_g)/\Delta H_m$ versus $T_g/T_m$ (calculated and proposed here) for a series of glass-forming oxides, where three regions can be observed: the red area depicts the region and oxide glasses for which internal homogeneous crystal nucleation is readily observed; the region of the two glasses for which no crystallisation is observed is blue. All the other points refer to oxide glasses that only crystallise heterogeneously starting on their external surfaces. This plot is in agreement with and reinforces Turnbull's[16] observation that liquids with $T_g/T_m > 2/3$ can be easily undercooled to the glassy state if they are free of crystalline seeds.

**Nucleus-Liquid Interfacial Energy ($\sigma_{cm}$).** Unfortunately the nucleus-melt interfacial energy, $\sigma_{cm}$, cannot be directly measured. However, it can be estimated using the Skapski–Turnbull[17–19] expression:

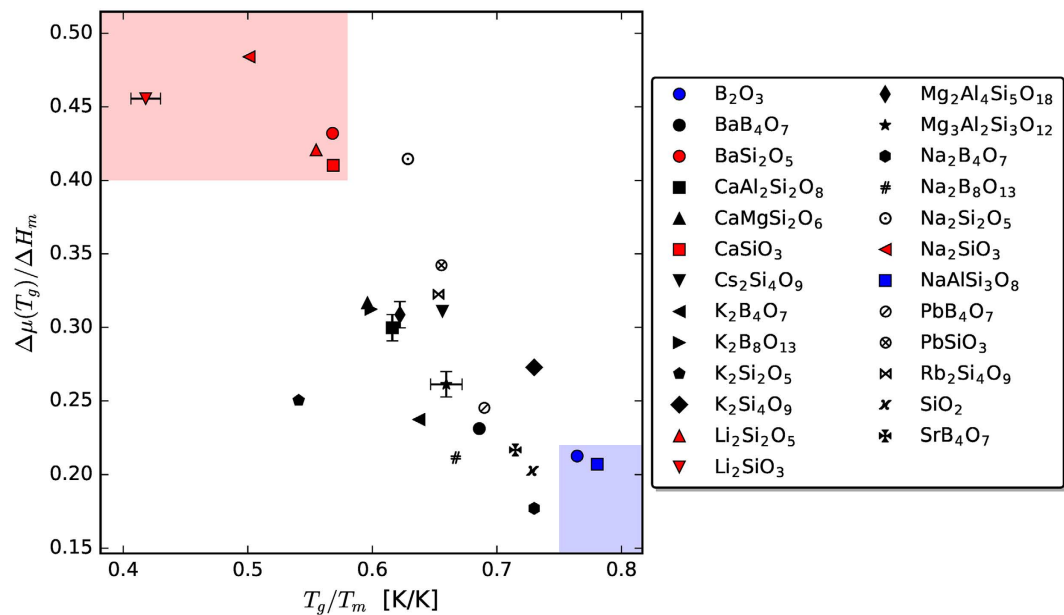$$\sigma_{cm} = \frac{\alpha\Delta H_m}{\sqrt[3]{N_A V_m^2}}, \tag{3}$$

**Figure 1. Reduced driving force for crystallisation evaluated at $T_g$ *versus* reduced $T_g$ for a number of oxide glass-formers.** The red points refer to compositions that reveal internal homogeneous crystal nucleation, whereas the blue points refer to the two known stoichiometric oxide liquids that do not show any signs of nucleation ($B_2O_3$ and Albite). The remaining points refer to supercooled liquids that only reveal surface (heterogeneous) crystal nucleation. When available, the typical uncertainties are shown for some compositions. Thermophysical data were obtained from various sources[46,47,63–76]. Values of $T_g$ were obtained by fitting viscosity data collected from the SciGlass database[77].

where $\alpha$ is a non-dimensional constant and $N_A$ is Avogadro's number. From both theoretical arguments and the fitting of the Classical Nucleation Theory equation to experimental crystal nucleation rates in oxide glass-formers that show measurable homogeneous nucleation, $\alpha$ is expected to be in the range of 0.4–0.6[20]. For glasses that do not display homogeneous nucleation $\alpha$ may be even higher.

**Viscosity and Diffusivity.** The effective diffusion coefficient controlling viscous flow and supposedly crystal nucleation and growth in supercooled liquids can be calculated by the Eyring[21] equation:

$$D_\eta = \frac{k_B T}{d\eta},$$
(4)

where $D_\eta$ is the diffusion coefficient, $k_B$ is Boltzmann's constant, $d$ is the jump distance, which is equivalent to the diameter of the diffusing molecules, and $\eta$ is the viscosity. As $d$ varies significantly less with temperature than $\eta$, for practical purposes it can be considered a constant equal to $d_o \sim (V_m/N_A)^{1/3}$.

Several viscosity equations are available in the literature[22–25]. In this work we considered the VFT[26–28] which corresponds to Eq. (5). This equation together with Eq. (6) (also known as CWAM[29,30]) fit the viscosity data of oxide liquids between the $T_g$ and $T_m$ very well, but yield <u>upper</u> and <u>lower</u> bounds, respectively, for the extrapolated values of the equilibrium viscosity below $T_g$. They are both used in this article.

$$\log_{10}(\eta) = \log_{10}(\eta_{\infty,VFT}) + \frac{C_{VFT}}{T - T_0}$$
(5)

$$\log_{10}(\eta) = \log_{10}(\eta_{\infty,CWAM}) + \left(\frac{A}{T}\right)^{B}$$
(6)

In these equations, $\eta_\infty$ is the asymptotic value of the equilibrium viscosity when $T \to \infty$, and A, B, C, and $T_0$ are adjustable parameters. Figure 2 shows viscosity data and fitted curves for Albite and $B_2O_3$ in an Oldekop–Laughlin–Uhlmann–Angell[31–33] (OLUA) plot. The values for the adjustable parameters in this figure are shown in Table 1.

The actual diffusion coefficients controlling crystal nucleation and growth, $D_I$ and $D_U$, respectively, are unknown for oxide glass formers. Hence they have been largely calculated by the Eyring or Stokes-Einstein equations, $D_\eta$[34–39], which yield good results for various oxide glass formers[38] at relatively high temperatures not far below the *liquidus*. Accurate crystal growth studies revealed that this equation breaks down at deep supercoolings, at $T_d \sim 1.1$–$1.2 T_g$[38,39]. Equilibrium viscosity and crystal growth kinetics are thus "coupled" from the melting point down to $T_d$, but they diverge significantly below $T_d$. For this reason, $T_d$ is often denominated decoupling
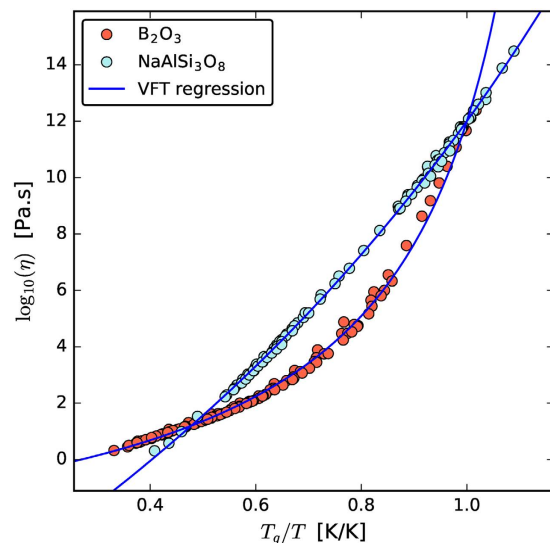
3

**Figure 2. Viscosity data for Albite[78–86] and B$_2$O$_3$[87–90] and fitted curves using the VFT equation.** These are examples of "strong", almost linear (Albite) and "fragile", highly curved (B$_2$O$_3$) liquids.

|  | $\eta_{\infty,\text{VFT}}$ (Pa.s.) | $C_{\text{VFT}}$ (K) | $T_0$ (K) | $\eta_{\infty,\text{CWAM}}$ (Pa s) | A (K) | B | $T_g$ (K) |
|---|---|---|---|---|---|---|---|
| Albite | $10^{-5.44}$ | 12,700 | 356 | −3.25 | 9,302 | 1.66 | 1,085 |
| B$_2$O$_3$ | $10^{-0.97}$ | 1,580 | 433 | 0.55 | 1,270 | 3.90 | 551 |

**Table 1. Fitted values of the viscosity parameters for both liquids.** $T_g$ is defined here as the temperature where the viscosity is equal to $10^{12}$ Pa.s.

(or breakdown) temperature. However, to the best of our knowledge, signs of a similar breakdown of the crystal nucleation kinetics have not been clearly shown to-date. Therefore, in this article, we use the Eyring equation to approximate the diffusion coefficient controlling nucleation, and thus neglect the effects of a (possible) breakdown. In addition, as the crystal growth calculations are carried out above $T_d$, as we will show later, there is no need to consider a (possible) breakdown. Finally, at least Albite is a very "strong" liquid for which the breakdown is much less likely.

## Theories and Models of Crystallisation and their Applicability

Crystallisation may be divided into the following two processes: the formation of stable crystalline nuclei, and their volume change with time and temperature. The first is termed crystal nucleation and the second is termed crystal growth. In the following subsections we will briefly introduce the main models for these two processes.

**Classical Nucleation Theory.** The Classical Nucleation Theory (CNT) provides the physical description of the crystal nucleation process. Here we introduce the basic equations for the steady-state homogeneous crystal nucleation rate, $I_{\text{st}}$,

$$I_{st} = I_0 \exp\left(-\frac{W_c}{k_B T}\right),$$

(7)

$$I_0 = \sqrt{\frac{\sigma_{cm}}{k_B T}} \frac{D_I}{d_0^4},$$

(8)

and the time-lag for crystal nucleation, $\tau$ (time necessary for the establishment of a stationary embryo size distribution up to the critical size),

$$\tau = \frac{16 k_B T \sigma_{cm}}{\pi \Delta \mu_V^2 d_0^2 D_I}.$$

(9)

For spherical nuclei, the work of the formation of a nucleus with a critical size, often denoted as the thermodynamic barrier for crystal nucleation, $W_c$ is given by Eq. (10).

$$W_c = \frac{16\pi V_m^2 \sigma_{cm}^3}{3\Delta\mu^2}$$

(10)

A nucleus is called "critical" when its growth is spontaneous resulting in a decrease of the system's Gibbs free energy. These relations will be used in the present study to estimate the crystal nucleation rates in the framework of CNT. In the above equations, $\sigma_{cm}$ is the crystal-liquid interfacial energy of the critical nucleus (in units of J/m$^2$, assumed to be the same used in the macroscopic growth equations); $k_B$ is the Boltzmann constant; $T$ is the absolute temperature; $\Delta\mu_v$ is the driving force for crystallisation in units of J/m$^3$; and $D_I$ is the effective diffusion coefficient determining the processes of aggregation of "structural units" to the crystalline clusters, estimated here by the Eyring expression (Eq. 4). Hence, the expression for the nucleation rate becomes

$$I_{st} = \sqrt{\frac{\sigma_{cm}}{k_B T}} \frac{k_B T}{d_0^5 \eta} \exp\left(-\frac{W_c}{k_B T}\right).$$

(11)

The actual <u>magnitudes</u> of $I_{st}$ cannot be calculated with a reasonable degree of accuracy due to the uncertainty in $\sigma_{cm}$[40,41] and its cubic exponent inside an exponential. However, the temperature dependence of $I_{st}$ and the location of its maximum, $T_{max}$, can be adequately calculated using properly estimated values of $\sigma_{cm}$, as we will do in this article.

Certain defect sites and solid impurities can reduce the thermodynamic barrier and the time-lag for nucleation. The formulation presented above can be maintained with correction factors[42] given by Eqs (12) to (15).

$$W_{c,het} = W_c \phi(\theta)$$

(12)

$$\phi(\theta) = \frac{1}{2} - \frac{3}{4} \cos(\theta) + \frac{1}{4} \cos^3(\theta)$$

(13)

$$\tau_{het} = \tau \xi(\theta)$$

(14)

$$\xi(\theta) = 1 - \frac{\cos(\theta)}{2} - \frac{\cos^2(\theta)}{2}$$

(15)

In the above equations, $W_{c,het}$ is the thermodynamic barrier for heterogeneous crystal nucleation, $\phi$ and $\xi$ are functions that depend on the contact angle between the nucleus and the substrate, $\theta$, and $\tau_{het}$ is the time-lag for heterogeneous nucleation.

A key parameter that can be measured for glass-forming systems is the nucleation time-lag, $\tau$, as a function of temperature, as shown in ref. 43. For all oxide glass-forming liquids tested to-date, these nucleation time-lags only become detectable (reach laboratory time scales) in the neighbourhood of their respective $T_g$ and keep increasing upon further supercooling.

Figure 3 shows the experimental values of $\tau$ at the temperatures of maximum crystal nucleation rate, $T_{max}$. These are data for 12 substances that show homogeneous nucleation in laboratory time scales. It is quite clear that $\tau$ increases dramatically (please note the logarithm scale) with increasing values of the reduced glass transition temperature $T_{gr} = T_g/T_m$. An extrapolation of this plot for the cases of Albite ($T_{gr} = 0.78$) and $B_2O_3$ ($T_{gr} = 0.76$) gives an estimated time-lag of more than $10^{10}$ seconds (about 300 years).

Figure 4(a) and (b) shows the cupola shape of the crystal nucleation rate curves for glassy Albite and $B_2O_3$. The homogeneous nucleation ($\theta = \pi$ rad, blue line) rate maxima are located well <u>below</u> the glass transition temperatures, which suggest that the crystal nucleation rates at and above $T_g$ (where the kinetic phenomena start to be measurable for most glass-forming systems) could be extremely small.

Compare these figures with Fig. 4(c), which shows experimental data and calculations for lithium disilicate (LS2), a supercooled liquid that undergoes internal homogeneous nucleation. The position of the *homogeneous* crystal nucleation peak for LS2 in the respective $T/T_m$ scale is not much different from the same peak for Albite, but the value of $T_g/T_m$ for LS2 is equal to its homogeneous crystal nucleation maximum. We will discuss this issue in more detail below.

Experimental data for heterogeneous crystal nucleation of LS2[44,45] in a supercooled liquid contained in a Pt pan is well described using a value of $\theta = \pi/7$ rad. When we used this value of $\theta$ in the calculations for Albite and $B_2O_3$ an interesting picture emerged: the *heterogeneous* nucleation peak is in fact well above the glass transition temperature for these two compositions, a temperature region where the expected nucleation time-lags are much shorter. This means that heterogeneous crystal nucleation may be possible in these materials with a powerful nucleation agent (such as seeding with their own isochemical crystals).

To calculate the nucleation curves of Fig. 4(a) and (b), we used Eq. (11) with $d_0$ calculated from the molar volume, as shown in Subsection 2.3. In this context we calculated $\sigma_{cm}$ via Eq. (3) with $\alpha = 0.5$ and $\Delta\mu_v$ by Eqs (1) and (2). Table 2 shows all the physical and thermodynamic parameters used in the calculations. The heat capacity for the crystalline phase is shown in Eq. (16) for Albite[46] and Eq. (17) for $B_2O_3$[47]:
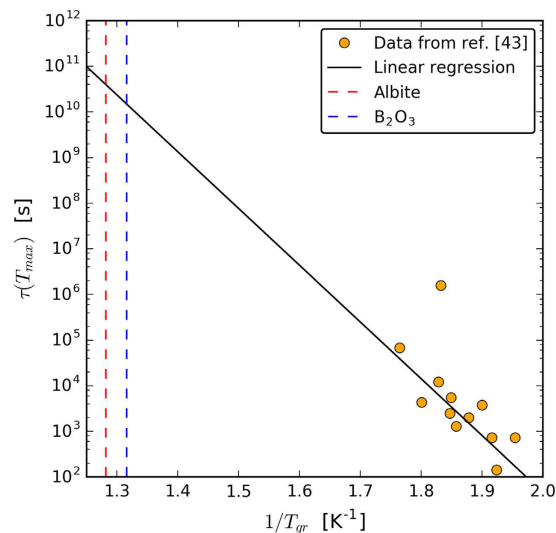
**Figure 3. Experimental values of the nucleation time-lags at $T_{max}$ for 12 oxide compounds that show homogeneous nucleation in laboratory time scales.** Data from ref. 43. The dashed vertical lines refer to the expected values for $B_2O_3$ and Albite from a linear extrapolation.

$$C_{p,c}(T) = \begin{cases} 258 + 0.058T - \dfrac{6280000}{T^2}, & T < 476 K \\ 343 + 0.015T - \dfrac{21000000}{T^2}, & T \geq 476 K \end{cases},$$

(16)

$$C_{p,c}(T) = 64.2 + 0.065T - \frac{1840000}{T^2} + 3 \times 10^{-8}T^2,$$

(17)

with $C_{p,c}$ in J/K.mol and T in Kelvin.

The values of equilibrium viscosity (rather than the non-equilibrium viscosity), given by Eq. (5) were used even below the $T_g$ of each glass because the structural relaxation times, $\tau_{rel}$, are significantly shorter than the crystal nucleation time-lags, which is similar to the average time of formation of the first critical nucleus, $<\tau>$. In fact, the temperature where $\tau_{rel} = <\tau>$ is the so-called supercooled liquid metastability limit (SCLML) or kinetic spinodal, $T_{KS}$[48–50]. Our estimates of $T_{KS}$ for three oxide liquids (to be published) demonstrate that $T_{KS}/T_m < 0.50$, whereas $T_{max}/T_m$ for Albite is 0.55 and is 0.65 for $B_2O_3$. Therefore, these two glasses should relax to the supercooled liquid state before the first critical nucleus is formed. Hence, the use of equilibrium viscosity to calculate nucleation kinetics above $T_{KS}$ is a very reasonable assumption. However, in any case, if instead the non-equilibrium viscosity were used in the calculations, the resulting $T_{max}$ would be located at even deeper supercoolings. In that case, the conclusion so far reached (long nucleation time-lags) would be reinforced. We have also used Eq. (6) for the equilibrium viscosity in the above discussed calculations and the results did not significantly change.

A key element for the rationale of the present article is that the maximum experimental steady-state homogenous crystal nucleation rates, $I_{st}(T_{max})$ drastically decrease with increasing $T_{gr}$ of the parent glass. The overall picture is shown in Fig. 5 and has also been corroborated by theoretical calculations as discussed thoroughly by Fokin *et al.*[43]. This figure indicates that the homogeneous nucleation rates in Albite ($T_{gr} \sim 0.78$) and $B_2O_3$ ($T_{gr} \sim 0.76$) are likely extremely small.

Apart from three outliers, the theoretical prediction is sufficient to describe all the other experimental data within the uncertainty (that is, the range considering $C_1$ from 5.0 to 6.5.) The data scatter makes it difficult to affirm that the temperature dependence of the theoretical prediction is different from the experimental data. Perhaps the experimental data show a steeper decrease than the theoretical prediction, but if this is the case, our conclusions would not be affected.

**Crystal Growth Models.** Experimental crystal growth rates in oxide glass-formers are reasonably well described by one of the following three classical models: *normal* or continuous growth, *screw dislocation* growth, and 2D *secondary nucleation growth*[20]. The first two growth modes are quite common for oxide glass-formers and share the same expression:

$$U = f\frac{D_U}{d_0}\left[1 - \exp\left(-\frac{\Delta\mu}{RT}\right)\right].$$

(18)

The difference between these two growth models is on the fraction of sites on the growing crystal interface available for atomic attachment, $f$. For materials with a small melting entropy[51], $\Delta H_m/T_m < 2R$ (R is the
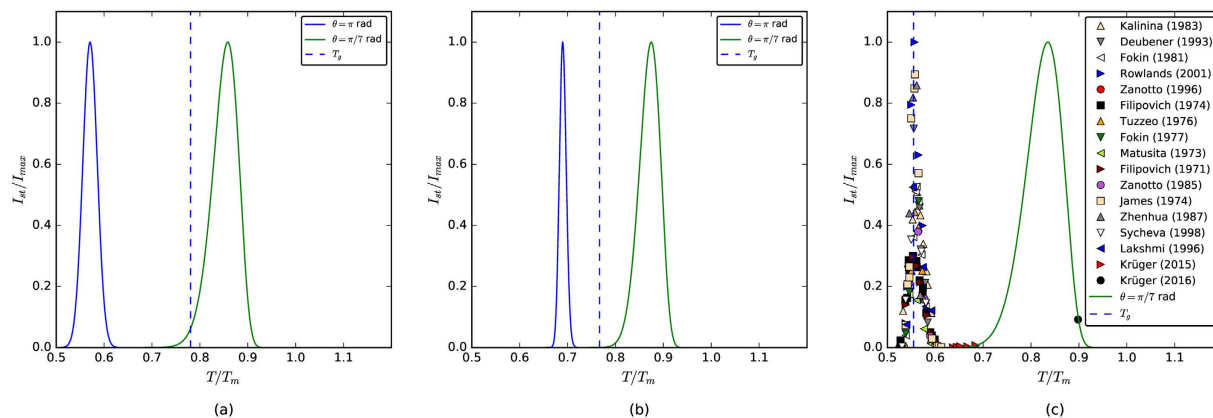
**Figure 4.** Normalized crystal nucleation rate curves *versus* reduced temperature for the cases of homogeneous nucleation ($\theta = \pi$ rad) and heterogeneous nucleation ($\theta = \pi/7$ rad) for (**a**) Albite and (**b**) $B_2O_3$. A plot for lithium disilicate is shown in (**c**) to compare our calculations for Albite and $B_2O_3$ with experimental homogeneous[91–104] and heterogeneous[44,45] crystal nucleation data. The value of $I_{max}$ for the heterogeneous crystal nucleation data was taken from Fig. 6 of ref. 45. The vertical dashed line is the estimated $T_g$ (where the viscosity is $10^{12}$ Pa.s.).
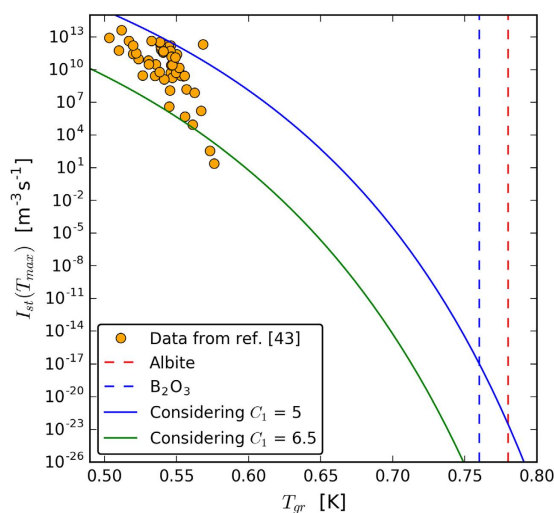


**Figure 5. Maximum experimental steady-state homogeneous crystal nucleation rates at $T_{max}$ *versus* reduced $T_g$ ($T_{gr}$) for 51 oxide glass-formers that undergo internal homogeneous nucleation.** Data from ref. 43. The full line is the predicted $I_{st}(T_{max})$ using Eqs (3), (9), (16) and (17) from Gupta *et al.*[105] In these calculations we considered reasonable values of $C_2 \equiv C_{VFT}/T_m = 4$, $I_0 = 10^{42}$ m$^{-3}$ s$^{-1}$, and $C_1 \equiv (\Delta\mu/\Delta H_m)^2 W_c/k_B T_m$ equal to 5.0 and 6.5. The vertical dashed blue line refers to the $T_{gr}$ of $B_2O_3$ and the red line to Albite.

|  | Albite | Source | $B_2O_3$ | Source | unit |
|---|---|---|---|---|---|
| $T_g$ | 1086 | viscosity | 554 | viscosity | K |
| $V_m$ | 100.3 | 106 | 27.3 | 107 | cm$^3$/mol |
| $d_0$ | 5.5 | calculated | 3.6 | calculated | Å |
| $T_m$ | 1391 | 73 | 723 | 47 | K |
| $\alpha$ | 0.5 | assumption | 0.5 | assumption | non-dimensional |
| $\Delta H_m$ | 59,300 | 108 | 24,070 | 47 | J/mol |
| $\sigma_{cm}$ | 0.16 | calculated | 0.16 | calculated | J/m$^2$ |
| $C_{p,l}$ | 369 | 75 | $128 - 0.0003T$ | 46 | J/K.mol |
| $C_{p,c}$ | Eq. (16) | 46 | Eq. (17) | 47 | J/K.mol |

**Table 2. Some properties of glassy and crystalline Albite and $B_2O_3$.**

gas constant), *f* is independent of the temperature and approximately 1. In such case, *normal* growth prevails. Otherwise, if $0 < f < 1$ and is temperature dependent, then the *screw dislocation* mechanism governs
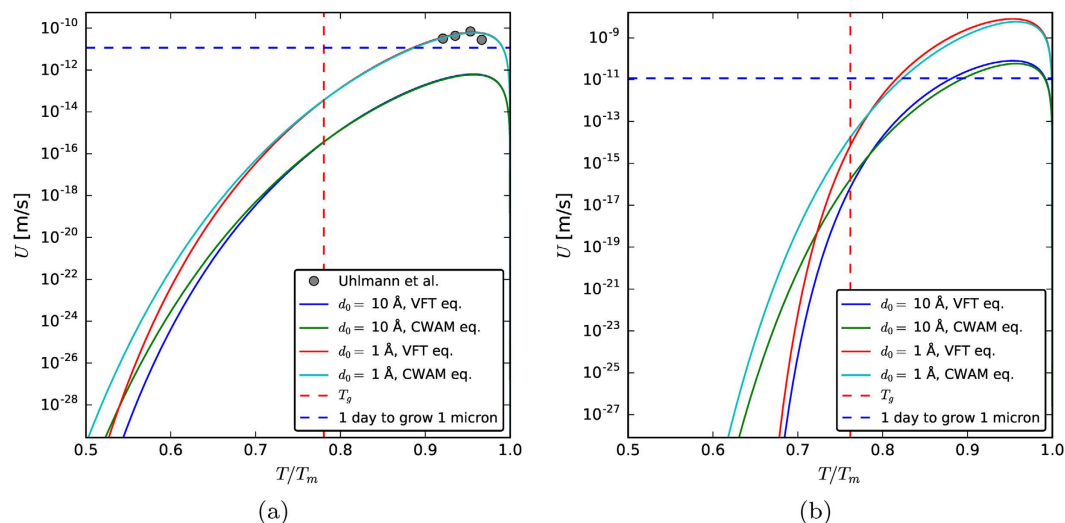
**Figure 6.** Simulations with the screw dislocation crystal growth model for (**a**) Albite and (**b**) $B_2O_3$. The experimental data points in (**a**), referring to the growth of crystalline layers in seeded Albite glass observed by Uhlmann *et al.*[10], match the curve calculated with $d_o = 1$ Å. The horizontal dashed line refers to the value of growth rate for which the crystals would grow $1\,\mu$m in 1 day.

crystal growth. The parameter $f$ can be estimated using Eq. (19) if one considers screw dislocations that form Archimedean spirals[52] at the advancing liquid–crystal interface.

$$f = \frac{d_0 \Delta \mu_V}{4\pi\sigma}$$

(19)

In the above equations, $U$ is the crystal growth rate, $D_U$ is the effective diffusion coefficient controlling crystal growth, and $\sigma$ is the crystal-liquid surface energy (normally assumed to be size and temperature independent and equal to $\sigma_{cm}$). When $f = 0$ (perfect crystals) then crystal growth must occur via 2D secondary nucleation, each crystal layer being formed by a secondary nucleus on the top of the primary nucleus and so on. The expression for this mechanism is well documented in Gutzow & Schmelzer's book[20].

To calculate the crystal growth rates curves shown in Fig. 6, we used Eqs (18) and (19) and the same value for $\sigma$ used in the Subsection 3.1 and two values for $d_0$, of the order of magnitude of a chemical bond length. The experimental data points refer to the growth of crystalline layers observed by Uhlmann *et al.*[10] after dusting an Albite glass surface with crystalline Albite mineral crystals.

Therefore to grow a crystal of 1 micron (that is resolvable under an optical microscope) one would need <u>many</u> years at the temperatures of maximum homogeneous nucleation, $T_{max} \sim 0.55T_m$ (Albite) and $\sim 0.65T_m$ for $B_2O_3$. However, for temperatures well above $T_g$, measurable growth occurs in a timeframe of hours, as shown in Fig. 6(a), where the four data points of Uhlmann *et al.*[10] (obtained with seeded Albite glass) fit quite well the calculated curve with $d_0 = 1$ Å. In summary, the maximum <u>crystal growth</u> rates are slow ($U_{max} \sim 1$ Å/s for Albite and $\sim 50$ Å/s for $B_2O_3$), but growth can and has been observed above $T_g$ and is not the problem hindering the crystallisation in supercooled Albite liquid, as shown by the experiments with seeded samples[10–12]. For $B_2O_3$ the theoretically estimated growth rates (by the screw dislocation mechanism) are even higher than those of Albite. However, we cannot draw firm conclusions about its growth kinetics because, to our knowledge, no published growth data are available for growth of $B_2O_3$ crystals at ambient pressure. One could also argue the growth rates in this glass could be described by another growth mechanism.

In any case, the exceptional resistance to crystallisation of both liquids clearly resides in their poor crystal <u>nucleation</u> kinetics, which was theoretically analyzed in the preceding sessions. In the following session, we dwell on the structures of the glass and their isochemical crystal phases in a quest for a structural reason for this poor nucleation ability.

## Structural Aspects of the Glasses and their Isochemical Crystals

It is known empirically[53] that the densities of the parent glass and corresponding crystal phase are quite similar ($\Delta\rho/\rho_{glass} < 8\%$) for all stoichiometric oxide glasses that display internal homogeneous crystal nucleation in laboratory time/size scales. However, several stoichiometric oxide glasses that only display surface (heterogeneous) nucleation, or no nucleation at all, show higher values of $\Delta\rho/\rho_{glass}$. In the case of Albite, $\Delta\rho/\rho_{glass} = 15\%$ and for $B_2O_3$ the density mismatch is approximately 34%.

The $\Delta\rho/\rho_{glass}$ ratio gives clear signs of structural similarity or dissimilarity between the parent glass and its isochemical crystal, hence Albite and $B_2O_3$ seem to have a significantly different structure from their crystalline phases. Let us consider two extreme cases: if the structure of the liquid is very close to that of its crystal form, then their densities must be similar and the necessary structural reorganization for crystallisation is facilitated by

the reduction in the kinetic barrier for nucleation and reduction of the surface energy, but the thermodynamic driving force, $\Delta\mu_V$, will be weak. However, as the crystal nucleation rates exponentially diminish with an increase in $\sigma_{cm}^3/\Delta\mu_V^2$ (Eq. 10), the role of $\sigma_{cm}$ is stronger and prevails. Structural similarity (lower $\sigma_{cm}$) is thus favourable for higher nucleation rates. The cases of Albite and $B_2O_3$, for which the densities (and inferentially the structures) of the liquids strongly differ from those of the isochemical crystals, correspond to a high surface energy, which lead to smaller nucleation rates. As the values of $\alpha$ (Eq. 3) are unknown for glasses displaying heterogeneous nucleation, we cannot estimate the values of the surface energy for these two glasses.

However, other oxide glasses also have similar high values of density mismatch and still crystallise, although they always do with the crystal growth starting on heterogeneous nucleation sites that exist on the sample surfaces[54]. Hence, this large density mismatch is only an indication of the structural dissimilarity. One should then dive deeper into the structural details of the parent glass and crystal phases for further insight, as we will indeed do below.

### Structures of Albite Glass and Crystal.

Ordering at short-length and, in some cases, at intermediate-length scales is a universal feature of the glassy state. Taylor and Brown[55] indicated that the structure of Albite glass consists predominantly of 6-membered Si–O rings, whereas the structure of the isochemical crystalline compound is exclusively constructed of 4-membered rings.

According to Zanotto *et al.*[54] the dipolar second moments, $\Delta M_2/M_{2C}$, describing the spatial correlation between the network modifiers in oxide glasses and their isochemical crystals vary from approximately 4 to 16% for oxide systems that undergo internal homogenous crystal nucleation, whereas for those which only display surface nucleation, this parameter may reach 60%. However, for Albite glass and crystals, the Na-Na second moment differs by more than 130%! This is by far the largest difference ever reported for the modifier-modifier second moment among all oxide glass formers and clearly points to significant structural differences between the glass and crystal phases.

These results further support our working hypothesis that the intermediate and medium range structure of Albite glass and its corresponding crystal phase widely differ. However, this significant structural difference seems to hinder crystal nucleation only in said composition, not crystal growth, because Uhlmann *et al.*[10], Selvaraj *et al.*[11], and Liu *et al.*[12] were able to crystallise Albite glass at high temperatures using crystalline seeds. This insensitiveness of crystal growth to the structural mismatch results from growth being normally measured at much higher temperatures ($T \sim T_m$) where bond breaking and rearrangement is much easier than at deep supercoolings, $T \sim T_g$, where the nucleation rates are normally measured.

### Structures of $B_2O_3$ Glass and Crystal.

High-resolution nuclear magnetic resonance (NMR) measurements of Oxygen-17 in $B_2O_3$ glass[56] provided evidence for structural units responsible for ordering on short- and intermediate-length scales. At the molecular level, planar $BO_{3/2}$ units accounted for the local ordering. Oxygen-17 NMR spectra resolved detailed features of the inclusion of these units in boroxol rings, oxygen bridging two rings, and oxygen shared between two nonring $BO_{3/2}$ units. On the basis of these and corroborative boron-11 NMR and scattering results, the authors concluded that boron oxide glass consists of domains that are rich or poor in boroxol rings. Approximately 70% of the boron atoms are located in boroxol-rich regions. The radius of the ring-rich domains was estimated to be about 20 Å or larger, which is quite similar to the sizes proposed from independent light scattering experiments and the Boson peak observed in Raman spectra. These domains were proposed to be the structural basis of intermediate-range order in glassy boron oxide.

A not yet well understood question is the relationship between the glassy and the various possible crystalline forms a system may adopt. By means of *ab initio* calculations, Ferlat *et al.*[57] discovered the existence of $B_2O_3$ crystalline polymorphs with structural properties similar to the glass and formation energies comparable to the known ambient crystal. According to those authors, the energy degeneracy of the crystals, which is high at ambient pressure and suppressed under pressure, provides a framework to understand the system's ability to vitrify and the origin of the crystallisation anomaly. Their main contribution was to evidence these novel crystals, some of them sharing greater structural similarity with the glass than do the experimentally synthesized crystals ($B_2O_3$-I). The ease of vitrification of $B_2O_3$ was related to the competition for crystallisation between numerous low-energy crystals (some with boroxols, some without). The authors considered that their work reaffirms the role played by polymorphism in a system's ability to vitrify[58,59].

From an experimental perspective, 80 years ago Kracek *et al.*[60] prepared a $B_2O_3$ glass sample sprinkled with $B_2O_3$-I crystal seeds (this phase is not explicitly stated in their paper, but this is in agreement with its reported melting point of 450 °C). After several months at various temperatures, the crystals remained suspended and did not grow. As far as we know, no one has ever tried to seed $B_2O_3$ glass with $B_2O_3$-II crystals, but then the density mismatch would be even higher (3.11 g/cm³, giving almost 70% difference) or other polymorphs.

One important remark is that the structure of $B_2O_3$-I is exclusively made by $BO_3$ triangles[61], which is significantly different from the $\sim 70\%$ boroxol rings that the glass is made. In a recent publication, Wright and Vedisheva[62] suggested that the excellent glass-forming ability of $B_2O_3$ is due to the need to either break up the boroxol groups to form crystalline $B_2O_3$-I, which has a structure based on ribbons of independent BO3 triangles, or to break up and reform boroxol groups to yield a suggested, but so far undiscovered, ambient pressure crystalline polymorph with a structure based solely on boroxols[62].

This finding for the inorganic oxide glass-formers Albite and $B_2O_3$ is analogous to what is known by the polymer science community. A few high molecular weight organic materials, in particular atactic polymers (e.g., polystyrene and PMMA) are very resistant to crystallisation because their intricate chain entanglements prevent the required molecular reorientation to organize themselves into a crystalline lattice.

| Parameter | Homogeneous nucleation | Albite | $B_2O_3$ | LS2 |
|---|---|---|---|---|
| $T_{gr}$ | $<0.60$ | 0.78 | 0.76 | 0.56 |
| Viscosity at $T_{max,homo}$ ($\theta = \pi$ rad) [Pa.s.] | $\leq 10^{12}$ Pa.s. | $\sim 10^{24}$ | $\sim 10^{23}$ | $\sim 10^{12}$ |
| Viscosity at $T_{max,hetero}$ ($\theta = \pi/7$ rad) [Pa.s.] | $<10^{12}$ Pa.s. | $\sim 10^{10}$ | $\sim 10^{7}$ | $\sim 10^{3}$ |
| $\Delta G(T_g)/\Delta H_m$ | $>0.4$ | $<0.2$ | $<0.2$ | 0.42 |
| $\Delta\rho/\rho_{glass}$ [%] | $<8$ | 15 | 34 | 4.3 |

**Table 3. Physical parameters controlling crystal nucleation in oxide glass formers that undergo homogeneous nucleation in comparison to Albite, $B_2O_3$, and LS2.**

**Summary of Properties and Structural Aspects.** Table 3 summarizes the main parameters that control the crystal nucleation rates. They are quite unfavourable for the two oxide glasses vindicating our hypothesis to explain the lack of observable crystallisation in these glasses.

Finally, it is quite interesting to note that Albite liquid is *strong*; its fragility index $m$ is 26. However, other strong liquids, such as $SiO_2$ and $GeO_2$ easily crystallise when heated above $T_g$. On the other hand, $B_2O_3$ can be considered a fragile glass-former ($m \sim 50$) and is also notoriously reluctant to crystallise, whereas many other fragile liquids easily crystallise. Hence, the abnormal crystal nucleation behaviour is not linked to the liquid fragility.

## Conclusions

Our analysis clearly demonstrates that the lack of detectable crystallisation ("crystallisation anomaly") in both supercooled liquids is indeed meagre homogeneous crystal nucleation, solving an enigma that persisted for 80 decades since the pioneering work of Kracek. This scenario is linked to the relatively small supercoolings where the glass transition takes place ($T_g/T_m = 0.76–0.78$) in these compositions. The latter leads to a very small crystallisation driving force at $T \geq T_g$, where crystallisation is normally observable in laboratory timescales. Thus, a deeper supercooling is necessary to achieve a high enough crystallisation driving force, leading to a $T_{max}$ that is well below the respective $T_g$. Associated with this, we demonstrated that the crystal nucleation time-lags are extremely long at $T_{max}$, effectively prohibiting that such experiments be conducted in laboratory time scales. However, for heterogeneous crystal nucleation catalysed by efficient nucleating agents, $T_{max}$ is shifted to higher temperatures above the respective $T_g$. In this setting, the predicted nucleation time-lags become measurable. These calculations explain the experimental results confirming that these glasses can be crystallised only when seeded with powerful nucleating agents. In the unseeded and ambient pressure conditions, they will only crystallise in geological time scales.

Moreover, this anomalous crystallisation behaviour is not linked with the liquid fragility, as both strong (Albite) and fragile ($B_2O_3$) liquids demonstrate this phenomenon. Ultimately, the major differences in the atomic structures of the parent liquids and their isochemical crystal phases are the cause for poor nucleation.

From a broader scientific and technological perspective, the present results not only debunk a long-standing mystery regarding the crystallisation anomaly, but also provide further insight into the connection between the structure and crystal nucleation ability of two important oxide glass forming liquids. In addition, these results could be used by glass researchers and engineers for the compositional design of oxide glasses that are stable against crystallisation. To that end, oxide glass-forming compositions should be selected that have a large $\Delta\rho/\rho_{glass}$ and large $T_g/T_m$.

## References

1. Debenedetti, P. G. & Stillinger, F. H. Supercooled liquids and the glass transition. *Nature* **410,** 259–267 (2001).
2. Zanotto, E. D. A bright future for glass-ceramics. *Am. Ceram. Soc. Bull.* **89,** 19–27 (2010).
3. Montazerian, M. *et al.* Bioactivity and cell proliferation in radiopaque gel-derived CaO-$P_2O_5$-$SiO_2$-$ZrO_2$ glass and glass–ceramic powders. *Mater. Sci. Eng. C* **55,** 436–447 (2015).
4. Montazerian, M. *et al.* Sol–gel synthesis, structure, sintering and properties of bioactive and inert nano-apatite–zirconia glass–ceramics. *Ceram. Int.* **41,** 11024–11045 (2015).
5. Mauro, J. C. & Zanotto, E. D. Two centuries of glass research: historical trends, current status, and grand challenges for the future. *Int. J. Appl. Glass Sci.* **5,** 313–327 (2014).
6. Schairer, J. F. & Bowen, N. L. The system $Na_2O$-$Al_2O_3$-$SiO_2$. *Am. J. Sci.* **254,** 129–195 (1956).
7. Uhlmann, D. R. In *Advances in nucleation and crystallization in glasses* (eds Hench, L. L. & Freiman, S. W.) 5, 91–115 (American Ceramic Society, 1972).
8. Uhlmann, D. R., Hays, J. F. & Turnbull, D. The effect of high pressure on $B_2O_3$: crystallisation, densification, and the crystallisation anomaly. *Phys Chem Glas.* **8,** 1–10 (1967).
9. Aziz, M. J., Nygren, E., Hays, J. F. & Turnbull, D. Crystal growth kinetics of boron oxide under pressure. *J. Appl. Phys.* **57,** 2233 (1985).
10. Uhlmann, D. R., Yinnon, H. & Cranmer, D. Crystallization behavior of albite. In *Lunar and Planetary Science Conference* **11,** 1178–1180 (1980).
11. Selvaraj, U., Liu, C. L., Komarneni, S. & Roy, R. Epitaxial crystallization of seeded albite glass. *J. Am. Ceram. Soc.* **74,** 1378–1381 (1991).
12. Liu, C., Komarneni, S. & Roy, R. Crystallization of Anorthite-seeded Albite glass by solid-state epitaxy. *J. Am. Ceram. Soc.* **75,** 2665–2670 (1992).
13. Siqueira, R. L., Peitl, O. & Zanotto, E. D. On the crystallization of gel-derived albite ($NaAlSi_3O_8$): the most stable oxide glass. *J. Sol-Gel Sci. Technol.*, doi: 10.1007/s10971-016-4176-z (2016).
14. Kelton, K. F. In *Solid State Physics* (eds Ehrenreich, H. & Turnbull, D.) Volume 45, 75–177 (Academic Press, 1991).
15. Cassar, D. R. Crystallization Driving Force of Supercooled Oxide Liquids. *Int. J. Appl. Glass Sci.* **7,** 262–269 (2016).
16. Turnbull, D. Under what conditions can a glass be formed? *Contemp. Phys.* **10,** 473–488 (1969).

17. Skapski, A. S. The surface tension of liquid metals. *J. Chem. Phys.* **16,** 389–393 (1948).
18. Skapski, A. S. A theory of surface tension of solids—I application to metals. *Acta Metall.* **4,** 576–582 (1956).
19. Spaepen, F. In *Solid State Physics* (eds Turnbull, D. & Ehrenreich, H.) 47, 1–32 (Academic Press, 1994).
20. Gutzow, I. S. & Schmelzer, J. W. P. *The vitreous state: thermodynamics, structure, rheology, and crystallization* (Springer, 2013).
21. Eyring, H.Viscosity, plasticity, and diffusion as examples of absolute reaction rates. *J. Chem. Phys.* **4,** 283–291 (1936).
22. Adam, G. & Gibbs, J. H. On the temperature dependence of cooperative relaxation properties in glass-forming liquids. *J. Chem. Phys.* **43,** 139–146 (1965).
23. Angell, C. A. & Bressel, R. D. Fluidity and conductance in aqueous electrolyte solutions. Approach from the glassy state and high-concentration limit. I. Calcium nitrate solutions. *J. Phys. Chem.* **76,** 3244–3253 (1972).
24. Cohen, M. H. & Grest, G. S. Liquid-glass transition, a free-volume approach. *Phys. Rev. B* **20,** 1077–1098 (1979).
25. Kivelson, S. A., Zhao, X., Kivelson, D., Fischer, T. M. & Knobler, C. M. Frustration-limited clusters in liquids. *J. Chem. Phys.* **101,** 2391–2397 (1994).
26. Vogel, H. Das Temperatureabhängigketsgesetz der Viskosität von Flüssigkeiten. *Phys. Z.* **22,** 645–646 (1921).
27. Fulcher, G. S. Analysis of recent measurements of the viscosity of glasses. *J. Am. Ceram. Soc.* **8,** 339–355 (1925).
28. Tammann, G. & Hesse, W. Die Abhängigkeit der Viscosität von der Temperatur bie unterkühlten Flüssigkeiten. *Z. Für Anorg. Allg. Chem.* **156,** 245–257 (1926).
29. Cornelissen, J. & Waterman, H. I. The viscosity temperature relationship of liquids. *Chem. Eng. Sci.* **4,** 238–246 (1955).
30. Avramov, I. & Milchev, A. Effect of disorder on diffusion and viscosity in condensed systems. *J. Non-Cryst. Solids* **104,** 253–260 (1988).
31. Oldekop, V. W. Theoretische betrachtungen über die Zähigkeit von Gläsern. *Glas. Berichte* **30,** 8–14 (1957).
32. Laughlin, W. T. & Uhlmann, D. R. Viscous flow in simple organic liquids. *J. Phys. Chem.* **76,** 2317–2325 (1972).
33. Angell, C. A. In *Relaxation in complex systems* (eds Ngai, K. L. & Wright, G. B.) 3–12 (Naval Research Laboratory, 1985).
34. Nascimento, M. L. F., Ferreira, E. B. & Zanotto, E. D. Kinetics and mechanisms of crystal growth and diffusion in a glass-forming liquid. *J. Chem. Phys.* **121,** 8924–8928 (2004).
35. Nascimento, M. L. F. & Zanotto, E. D. Mechanisms and dynamics of crystal growth, viscous flow, and self-diffusion in silica glass. *Phys. Rev. B* **73,** 1–7 (2006).
36. Nascimento, M. L. F. & Zanotto, E. D. Diffusion processes in vitreous silica revisited. *Phys. Chem. Glas. - Eur. J. Glass Sci. Technol. Part B* **48,** 201–217 (2007).
37. Reinsch, S., Nascimento, M. L. F., Müller, R. & Zanotto, E. D. Crystal growth kinetics in cordierite and diopside glasses in wide temperature ranges. *J. Non-Cryst. Solids* **354,** 5386–5394 (2008).
38. Nascimento, M. L. F. & Zanotto, E. D. Does viscosity describe the kinetic barrier for crystal growth from the liquidus to the glass transition? *J. Chem. Phys.* **133,** 174701 (2010).
39. Nascimento, M. L. F., Fokin, V. M., Zanotto, E. D. & Abyzov, A. S. Dynamic processes in a silicate liquid from above melting to below the glass transition. *J. Chem. Phys.* **135,** 194703, 194703–17 (2011).
40. Fokin, V. M., Zanotto, E. D., Schmelzer, J. W. P. & Potapov, O. V. New insights on the thermodynamic barrier for nucleation in glasses: The case of lithium disilicate. *J. Non-Cryst. Solids* **351,** 1491–1499 (2005).
41. Fokin, V. M., Zanotto, E. D., Yuritsyn, N. S. & Schmelzer, J. W. P. Homogeneous crystal nucleation in silicate glasses: A 40 years perspective. *J. Non-Cryst. Solids* **352,** 2681–2714 (2006).
42. Gutzow, I. & Toschev, S. In *Advances in nucleation and crystallization in glasses* (eds Hench, L. L. & Freiman, S. W.) 5, 10–23 (American Ceramic Society, 1972).
43. Fokin, V. M., Zanotto, E. D. & Schmelzer, J. W. P. Homogeneous nucleation versus glass transition temperature of silicate glasses. *J. Non-Cryst. Solids* **321,** 52–65 (2003).
44. Krüger, S. & Deubener, J. Heterogeneous surface nucleation of lithium disilicate glass: An isothermal DSC study. *J. Non-Cryst. Solids* **417–418,** 45–51 (2015).
45. Krüger, S. & Deubener, J. The TTT Curves of the Heterogeneous and Homogeneous Crystallization of Lithium Disilicate – A Stochastic Approach to Crystal Nucleation. *Front. Mater.* **3** (2016).
46. Barin, I. *Thermochemical data of pure substances* 2, (VCH, 1995).
47. Chase, M. W. J. *NIST-JANAF thermochemical tables* (American Inst. of Physics, 1998).
48. Kauzmann, W. The nature of the glassy state and the behavior of liquids at low temperatures. *Chem. Rev.* **43,** 219–256 (1948).
49. Das, S. P. *Statistical physics of liquids at freezing and beyond* (Cambridge University Press, 2011).
50. Tanaka, H. Possible resolution of the Kauzmann paradox in supercooled liquids. *Phys. Rev. E* **68,** 011505 (2003).
51. Jackson, K. A., Uhlmann, D. R. & Hunt, J. D. On the nature of crystal growth from the melt. *J. Cryst. Growth* **1,** 1–36 (1967).
52. Burton, W.-K., Cabrera, N. & Frank, F. C. The growth of crystals and the equilibrium structure of their surfaces. *Philos. Trans. R. Soc. Lond. Ser. Math. Phys. Sci.* **243,** 299–358 (1951).
53. Zanotto, E. D. & Muller, E. A simple method to predict the nucleation mechanism in glass. *J. Non-Cryst. Solids* **130,** 220–221 (1991).
54. Zanotto, E. D., Tsuchida, J. E., Schneider, J. F. & Eckert, H. Thirty-year quest for structure–nucleation relationships in oxide glasses. *Int. Mater. Rev.* **60,** 376–391 (2015).
55. Taylor, M. & Brown, G. E. Structure of mineral glasses—I. The feldspar glasses $NaAlSi_3O_8$, $KAlSi_3O_8$, $CaAl_2Si_2O_8$. *Geochim. Cosmochim. Acta* **43,** 61–75 (1979).
56. Youngman, R. E., Haubrich, S. T., Zwanziger, J. W., Janicke, M. T. & Chmelka, B. F. Short-and intermediate-range structural ordering in glassy boron oxide. *Science* **269,** 1416–1420 (1995).
57. Ferlat, G., Seitsonen, A. P., Lazzeri, M. & Mauri, F. Hidden polymorphs drive vitrification in $B_2O_3$. *Nat. Mater.* **11,** 925–929 (2012).
58. Wang, R. & Merz, M. D. Non-crystallinity and polymorphism in elemental solids. *Nature* **260,** 35–36 (1976).
59. Goodman, C. H. L. Strained mixed-cluster model for glass structure. *Nature* **257,** 370–372 (1975).
60. Kracek, F. C., Morey, G. W. & Merwin, H. E. The system, water-boron oxide. *Am. J. Sci.* **35A,** 143–171 (1938).
61. Strong, S. L., Wells, A. F. & Kaplow, R. On the crystal structure of $B_2O_3$. *Acta Crystallogr. B* **27,** 1662–1663 (1971).
62. Wright, A. C. & Vedishcheva, N. M. Borate networks: rigidity versus dimensionality. *Phys. Chem. Glas. Eur. J. Glass Sci. Technol. Part B* **57,** 1–14 (2016).
63. Asano, M. & Kou, T. Thermochemical properties of $BaBO_2(g)$ and $Ba_3B_2O_6(s)$. *J. Chem. Thermodyn.* **21,** 837–845 (1989).
64. Bosenick, A., Geiger, C. A. & Cemič, L. Heat capacity measurements of synthetic pyrope-grossular garnets between 320 and 1000 K by differential scanning calorimetry. *Geochim. Cosmochim. Acta* **60,** 3215–3227 (1996).
65. Kerr, E. C., Hersh, H. N. & Johnston, H. L. Low temperature heat capacities of inorganic solids. II. the heat capacity of crystalline boric oxide from 17 to 300 K. *J. Am. Chem. Soc.* **72,** 4738–4740 (1950).
66. Knacke, O., Kubaschewski, O. & Hesselmann, K. *Thermodynamic properties of inorganic substances* (Springer, 1991).
67. Krupka, K. M., Hemingway, B. S., Robie, R. A. & Kerrick, D. M. High-temperature heat capacities and derived thermodynamic properties of anthophyllite, diopside, dolomite, enstatite, bronzite, talc, tremolite, and wollastonite. *Am. Mineral.* **70,** 261–271 (1985).
68. Landolt-Börnstein. *Thermodynamic properties of inorganic material, scientific group thermodata europe (SGTE)* (Springer-Verlag, 1999).

69. Lenoir, M., Grandjean, A., Linard, Y., Cochain, B. & Neuville, D. R. The influence of Si,B substitution and of the nature of network-modifying cations on the properties and structure of borosilicate glasses and melts. *Chem. Geol.* **256,** 316–325 (2008).
70. Paukov, I. E., Kovalevskaya, Y. A., Rahmoun, N.-S. & Geiger, C. A. A low-temperature heat-capacity study of synthetic anhydrous Mg-cordierite ($Mg_2Al_4Si_5O_{18}$). *Am. Mineral.* **91,** 35–38 (2006).
71. Richet, P., Bottinga, Y., Denielou, L., Petitet, J. P. & Tequi, C. Thermodynamic properties of quartz, cristobalite and amorphous $SiO_2$: drop calorimetry measurements between 1000 and 1800 K and a review from 0 to 2000 K. *Geochim. Cosmochim. Acta* **46,** 2639–2658 (1982).
72. Richet, P. & Bottinga, Y. Anorthite, andesine, wollastonite, diopside, cordierite and pyrope: thermodynamics of melting, glass transitions, and properties of the amorphous phases. *Earth Planet. Sci. Lett.* **67,** 415–432 (1984).
73. Robie, R. A. & Hemingway, B. S. *Thermodynamic properties of minerals and related substances at 298.15 K and 1 bar ($10^5$ pascals) pressure and at higher temperatures* (U.S. G.P.O., 1995).
74. Smith, G. S. & Rindone, G. E. High-temperature energy relations in the alkali borates: binary alkali borate compounds and their glasses. *J. Am. Ceram. Soc.* **44,** 72–78 (1961).
75. Stebbins, J. F., Carmichael, I. S. E. & Weill, D. E. The high temperature liquid and glass heat contents and the heats of fusion of diopside, albite, sanidine and nepheline. *Am. Mineral.* **68,** 717–730 (1983).
76. Stewart, D. R. & Rindone, G. E. High-temperature energy relations in borates: alkaline-earth and lead borate compounds and their glasses. *J. Am. Ceram. Soc.* **46,** 593–596 (1963).
77. Mazurin, O. V. & Priven, A. I. SciGlass (*Glass Property Information System*) (ITC, Inc., 2013).
78. Sipp, A. & Richet, P. Equivalence of volume, enthalpy and viscosity relaxation kinetics in glass-forming silicate liquids. *J. Non-Cryst. Solids* **298,** 202–212 (2002).
79. Sipp, A., Bottinga, Y. & Richet, P. New high viscosity data for 3D network liquids and new correlations between old parameters. *J. Non-Cryst. Solids* **288,** 166–174 (2001).
80. Hummel, W. & Arndt, J. Variation of viscosity with temperature and composition in the plagioclase system. *Contrib. Mineral. Petrol.* **90,** 83–92 (1985).
81. Neuville, D. R. & Richet, P. Viscosity and entropy of liquid mixtures in the $SiO_2$-$Al_2O_3$-CaO-MgO system. *Riv. Della Stazione Sper. Vetro* **20,** 213–220 (1990).
82. Toplis, M. J., Dingwell, D. B., Hess, K.-U. & Lenci, T. Viscosity, fragility, and configurational entropy of melts along the join $SiO_2$-$NaAlSiO_4$. *Am. Mineral.* **82,** 979–990 (1997).
83. Kôzu, S. & Kani, K. Viscosity measurements of the ternary system diopside-albite-anorthite at high temperatures. *Proc. Imp. Acad.* **11,** 383–385 (1935).
84. Urbain, G., Bottinga, Y. & Richet, P. Viscosity of liquid silica, silicates and alumino-silicates. *Geochim. Cosmochim. Acta* **46,** 1061–1072 (1982).
85. Kani, K. Viscosity phenomena of the system $KAlSi_3O_8$-$NaAlSi_3O_8$ and of perthite at high temperatures. *Proc. Imp. Acad.* **11,** 334–336 (1935).
86. Scarfe, C. M. & Cronin, D. J. Viscosity-temperature relationships of melts at 1 atm in the system diopside-albite. *Am. Mineral.* **71,** 767–771 (1986).
87. Dietzel, A. & Brückner, R. Aufbau eines Absolutviskosimeters für hohe Temperaturen und Messung der Zähigkeit geschmolzener Borsäure für Eichzwecke. *Glas. Ber* **28,** 455–467 (1955).
88. Eppler, R. A. Viscosity of molten $B_2O_3$. *J. Am. Ceram. Soc.* **49,** 679–680 (1966).
89. Sugai, M. & Somiya, S. Measurement of density, viscosity and surface tension of the melt of the system $SiO_2$-$TiO_2$-$Al_2O_3$ at 1600 °C. *J. Ceram. Assoc. Jpn.* **90,** 262–269 (1982).
90. Moynihan, C. T. Correlation between the width of the glass transition region and the temperature dependence of the viscosity of high-tg glasses. *J. Am. Ceram. Soc.* **76,** 1081–1087 (1993).
91. Deubener, J., Brückner, R. & Sternitzke, M. Induction time analysis of nucleation and crystal growth in di- and metasilicate glasses. *J. Non-Cryst. Solids* **163,** 1–12 (1993).
92. Filipovich, V. N. & Kalinina, A. M. Relation between the vitrification temperature and the temperature of maximum rate of crystal nucleous formation in glasses. *Izv. Akad. Nauk SSSR Neorganicheskie Mater.* **7,** 1844–1848 (1971).
93. Fokin, V. M., Filipovich, V. N. & Kalinina, A. M. Investigation of the influence of preliminary heat treat ment of the $Li_2O \cdot 2SiO_2$ glass on the nucleation of crystals in it. *Fiz Khim Stekla* **3,** 129–136 (1977).
94. Fokin, V. M., Kalinina, A. M. & Filipovich, V. N. Nucleation in silicate glasses and effect of preliminary heat treatment on it. *J. Cryst. Growth* **52,** Part 1, 115–121 (1981).
95. James, P. F. Kinetics of crystal nucleation in lithium silicate glasses. *Phys. Chem. Glas.* **15,** 95–105 (1974).
96. Kalinina, A. M., Sycheva, G. A. & Filipovich, V. N. Homogeneous and heterogeneous crystal nucleation in some silicate glasses. *Glastech. Berichte* **56,** 816–821 (1983).
97. Lakshmi Narayan, K., Kelton, K. F. & Ray, C. S. Effect of Pt doping on nucleation and crystallization in $Li_2O \cdot 2SiO_2$ glass: experimental measurements and computer modeling. *J. Non-Cryst. Solids* **195,** 148–157 (1996).
98. Matusita, K. & Tashiro, M. Rate of homogeneous nucleation in alkali disilicate glasses. *J. Non-Cryst. Solids* **11,** 471–484 (1973).
99. Rowlands, E. G. & James, P. F. Nucleation and crystal growth in the lithia-baria-silica system. In *Proceedings of the XIXth International Congress on Glass* 68–69 (Society of Glass Technology, 2001).
100. Sycheva, G. A. Surface energy at the crystal nucleus-glass interface in alkali silicate glasses. *Glass Phys. Chem.* **24,** 342–347 (1998).
101. Tuzzeo, J. J. *Effects of pressure on kinetics of crystal nucleation in lithium disilicate glass* (The Ohio State University, 1976).
102. Zanotto, E. D. & James, P. F. Experimental tests of the classical nucleation theory for glasses. *J. Non-Cryst. Solids* **74,** 373–394 (1985).
103. Zanotto, E. D. & Leite, M. L. G. The nucleation mechanism of lithium dissilicate glass revisited. *J. Non-Cryst. Solids* **202,** 145–152 (1996).
104. Zhenhua, Z. A study of kinetics on crystal nucleation in lithium silicate glass. *J. Chin. Ceram. Soc.* **2,** 003 (1987).
105. Gupta, P. K., Cassar, D. R. & Zanotto, E. D. On the variation of the maximum crystal nucleation rate temperature with glass transition temperature. *J. Non-Cryst. Solids* **442,** 34–39 (2016).
106. Tenner, T. J., Lange, R. A. & Downs, R. T. The albite fusion curve re-examined: New experiments and the high-pressure density and compressibility of high albite and $NaAlSi_3O_8$ liquid. *Am. Mineral.* **92,** 1573–1585 (2007).
107. Gurr, G. E., Montgomery, P. W., Knutson, C. D. & Gorres, B. T. The crystal structure of trigonal diboron trioxide. *Acta Crystallogr. B* **26,** 906–915 (1970).
108. Robie, R. A., Hemingway, B. S. & Fisher, J. R. Thermodynamic properties of minerals and related substances at 298.15 K and 1 bar ($10^5$ pascals) pressure and at higher temperatures. *US Geol. Surv. Bull* (1978).

## Acknowledgements

## Author Contributions

E.D.Z. proposed the concept and strategy for the research and the manuscript. D.R.C. performed all the calculations. Both contributed with the literature review and writing of the manuscript.

## Additional Information

**Competing financial interests:** The authors declare no competing financial interests.

**How to cite this article:** Zanotto, E. D. and Cassar, D. R. The microscopic origin of the extreme glass-forming ability of Albite and $B_2O_3$. *Sci. Rep.* **7**, 43022; doi: 10.1038/srep43022 (2017).

**Publisher's note:** Springer Nature remains neutral with regard to jurisdictional claims in published maps and institutional affiliations.